Stringer Peeling Effects at Stiffened Composite Panels in the Postbuckling Range

D. Hachenberg*
Deutsche Aerospace Airbus GmbH, Hamburg, Germany
and
H. Kossira†
Technical University, Braunschweig, Germany

Results of an experimental and analytical study of the postbuckling behavior of stiffened graphite-epoxy panels loaded in pure shear are presented. The postbuckling response and failure characteristics of the panels are described. Panels with one and two stiffeners were tested. Failure of all panels originated in a skin-stiffener interface region. A method of computing the forces in the interface region between the skin and the stiffener, using a special contact element within a nonlinear finite element code is described. Analytical results correlate well with typical postbuckling test results up to failure. Typical stress distributions within the skin-stiffener interface region were determined analytically. A failure criterion for peeling delamination based on interlaminar forces is presented.

Nomenclature

a	= unit basic vector
E_{11}, E_{22}, E_{33}	= Young's modulus
F_{cr}	= stiffener debonding load
G_{12}	= in-plane shear modulus
G_{13}, G_{23}	= out-of-plane shear modulus
h	= plate thickness
I_x, I_y	= bending moment of inertia
J_D	= torsional moment of inertia
k_{i3}	= spring stiffnesses
n_{i3}	= transverse tractions
S_{ij}, S_{ijkl}	= strength tensors
u_1, u_2, u_3	= displacement
β_{11}, β_{22}	= generalized bending strains
γ	= angle of shear
$\nu_{12}, \nu_{13}, \nu_{23}$	= Poisson's ratio
τ	= shear stress
Φ	= element shape function matrix
φ_1, φ_2	= rotation

Subscripts

b	= buckling limit
bo	= upper surface of bottom element
c	= compression
cr	= failure value
t	= tension
to	= lower surface of top element
1	= in-plane longitudinal direction
2	= in-plane transverse direction
3	= normal (out-of-plane) direction

Superscripts

co	= contact plane between elements
*	= denotes the surface of the panel

Introduction

THE postbuckling load-carrying capacity of primary aircraft structural components, such as stiffened panels, is generally very high. For this reason, and in order to reduce structural weight, a design philosophy is applied, permitting buckling up to some fraction of the ultimate load. The application of such a postbuckling concept on advanced composite structures is restricted due to the fact that the most common failure mode of composite stiffened panels in the postbuckling range is stiffener debonding. This failure often occurs far beyond the potential ultimate load. The amount of work done on postbuckling behavior of stiffened composite airframe members has mostly been limited to experimental or analytical investigations[1-7] of the global nonlinear response, not taking into account the effects at the skin-stiffener interface. Some investigators[8,9] concentrate on the calculation of the local three-dimensional stresses, but do not consider the influence of the global postbuckling deformations. When using two separated models for the global and local analysis,[10] the collocation of both systems becomes very difficult in the nonlinear postbuckled regime.

Thus, a theoretical and experimental investigation has been carried out to improve the understanding of the nonlinear response of stiffened composite panels with special regard to the debonding mechanism. Graphite-epoxy plates, integrally stiffened by one or two T-shaped stiffeners, were tested in a shear-frame. These specimens were produced with the typical skin thicknesses and stacking sequences of primary structures of transport aircraft. Shear panels usually have a very large postbuckling load carrying capacity at their disposal, and stringer debonding occurs even though the stiffener itself is not under external load. In the experimental program, the influence of the stringer torsional and bending stiffnesses on the skin buckling modes and stiffener debonding effects were studied in a series of tests. Improvements of the interlaminar strength can be reached by pinning the skin-stiffener region of the laminate with steel or titanium pins. Such methods have been examined with the result that no stiffener debonding could be observed up to the ultimate load of the plate. Interlaminar material properties (as there are peeling strength and critical pop-off forces) were evaluated by special test specimens and are also described in this article.

To predict the magnitude of debonding sensitivity due to skin-buckling, it is necessary to analyze the nonlinear response on one side and to cope with three-dimensional effects on the

other side. Three-dimensional stresses are responsible for delamination and debonding, as the interlaminar strengths-properties of laminated composites are rather poor in relation to the inplane ones. In the analytical model, a nonlinear finite element code is used for postbuckling analysis. Three-dimensional stress distributions at the skin-stiffener interface are determined numerically by the use of a special interface element. This allows the critical region, where the starting point of the delamination is situated, to be defined. Good correlations could be achieved between the test results and the theoretical predictions. Two failure criteria are presented for stringer debonding, one based on interlaminar tractions calculated by the interface element, and the other based on postbuckling generalized bending strains.

Theoretical Investigations

Numerical Method

The following buckling and postbuckling analysis of stiffened laminated plates is based on a nonlinear shell theory of the Mindlin type (first-order shear deformation plate theory), which is valid over a wide range of thickness ratios and for large deformations, but moderate rotations. A total Lagrangian formulation is used, i.e., the state of the deformed panel is expressed in terms of the initial state. The nonlinear differential equations of the shell theory are transformed into a set of algebraic equations by means of the finite element method (FEM). An in-house (IFL) developed finite element code (FiPPS[11,12]) which is based on a mixed variational principle, was used to derive a plate element for the idealization of the panel and the stringer cross section. A detailed description of the application of the mixed variational principle on nonlinear finite element formulations can be found in Refs. 11–13. The major advantage of the used mixed principle is the fact that simple structured element matrices are obtained, and only C^0 continuity is required.

Double Node Principle

At the mixed variational principle, both the kinematic relations and the equilibrium conditions are satisfied, i.e., both the displacement (primal) variables and generalized force (dual) variables are given equal importance in the variational process. Thus, interpolation functions have to guarantee interelement continuity of not only displacements and rotations but also stress resultants. This fact has limited the application of mixed elements to structures without any abrupt changes in stiffness and unramified ones. The displacement variables may be defined in a global coordinate system but the stress resultants have to be related to the element reference plane, and in the case of a structural ramification—if there is no double-node—a unique association of the stress resultants is not possible. Similar problems arise if a discrete load normal to the element plane is applied. In this case, the mixed element formulation effects in a smoothing of the transverse forces discontinuity.

To overcome those lacks of the mixed elements and to make use of their uncontested advantages at nonlinear calculations, a decoupling of the stress resultants has to be performed in those areas of the structure where abrupt changes occur. This can be achieved by attaching the force variables to separated nodes, e.g., arranging them at the interior of the element, then they don't take part in the interelement continuity conditions.

In this study, a family of mixed elements was developed with two separated nodes at coincident corner positions (double-node-element). One node holds the displacement variables (primal node) and the other one the stress variables (dual node). While the primal nodes all have to be coupled between the elements, the dual nodes can be coupled or not, according to the structural discontinuities or ramifications. The advantages of the mixed formulation are therefore retained. The number of unknowns compared to the conventional mixed

formulation grows when introducing additional uncoupled dual nodes at the locations of discontinuities. The system bandwidth of the double node elements are larger than those of the conventional mixed elements, which results in higher storage requirements. Moreover, an unfavorable numbering of nodes may lead increasingly to indefinite system matrices, which are generally possible when using mixed finite element models requiring special solution procedures.[13]

The application of a shear deformation theory in connection with bilinear shape functions usually causes convergence problems, and at mixed formulations it presents oscillating stress resultants. This phenomenon, known as the shear locking effect, results from a coupling between inplane and transverse shear terms with decreasing plate thickness caused by incompleteness of the displacement functions. The problem can be solved by applying a reduced selective integration technique, which means eliminating all those terms at the functions that may cause incorrect coupling. In the case of a flat plate with transverse shear flexibility, some simple modifications of the shape functions for the rotations will solve the shear locking problem. The integration order has to be reduced respectively in one direction, resulting in constant distributions of rotations with bilinear shape functions.

Interface Element

According to the three-dimensional effects at the skin-stiffener interface, a special contact element had to be developed. In displacement models, the skin-stiffener area can easily be idealized by overlaying two plate elements connecting them to the same nodes and—with regard to their real position—adding an offset vector, which effects their moments of inertia. Because there is only one reference plane, and the variables of both elements are related to it, only plane stress or plane strain conditions can be achieved. On the other hand, if using solid elements, the three-dimensional stresses can be calculated, but because the taper fraction must be limited in order to avoid degenerations, the number of elements and unknowns of the global structural model grows enormously. The aim for the calculation of the skin-stiffener debonding problem was to have a simple model for the nonlinear global postbuckling analysis, and a specific local three-dimensional idealization only at those locations and interfaces where three-dimensional stresses would affect the stiffener debonding. Based on the double-node mixed plate-element, this was achieved by attaching two different reference systems, one to the elements representing the skin and the other to those representing the stiffener-flange (Fig. 1). Both separated partial systems are then connected by interface elements which are

Plate-element: * 'double-node' mixed Mindlin-type
  * 8 nodes, 4 primal-, 4 dual nodes
  * primal variables: $u_1, u_2, u_3, \varphi_1, \varphi_2, \varphi_3$
  * dual variables: $n^{11}, n^{22}, n^{12}, m^{11}, m^{22}, m^{12}, q^1, q^2$
  * 56 element variables

Interface-element: * mixed continuous spring-type
  * 12 nodes, 8 primal-, 4 dual nodes
  * primal variables: $u_1, u_2, u_3, \varphi_1, \varphi_2, \varphi_3$
  * dual variables: n^{13}, n^{23}, n^{33}
  * 60 element variables
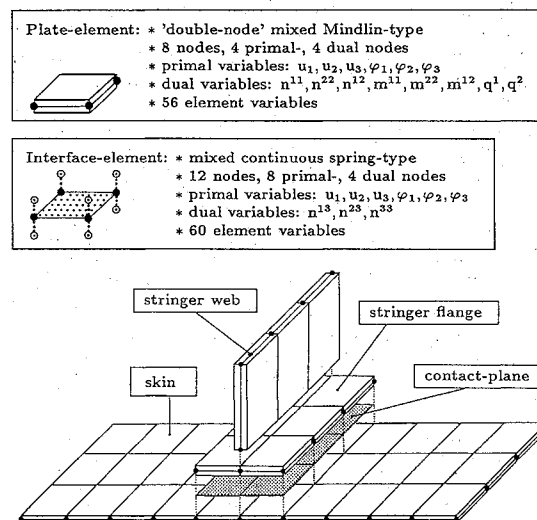
stringer web   stringer flange
skin   contact-plane

Fig. 1 Finite element idealization of a stiffened plate by Mindlin-type plate elements combined with an interface element.
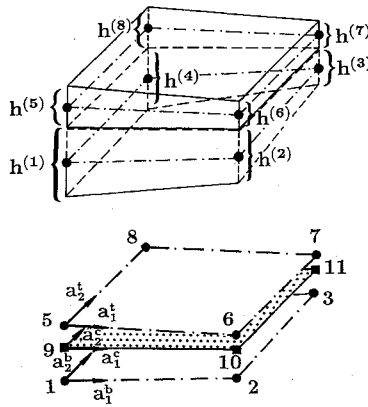
Fig. 2   Interface element as a joint between two plate elements.

based on linear spring models[14] using similar shape functions as those used for the connected plate elements.

Considering the 4-node plate element (Fig. 2) the displacements of any point at the bottom surface of the top element can be calculated by

$$[u_i^*]_{bo} = \sum_{k=1}^{4} \phi^{(k)}[u_i^{(k)}]_{bo} - \sum_{k=1}^{4} \phi^{(k)} \frac{h^{(k)}}{2} [-a_2^{bo} a_1^{bo}] \begin{bmatrix} \varphi_1^{(k)} \\ \varphi_2^{(k)} \end{bmatrix}_{bo} \quad (1)$$

In a similar way, the displacements at the lower surface of the top element read

$$[u_i^*]_{to} = \sum_{k=5}^{8} \phi^{(k)}[u_i^{(k)}]_{to} + \sum_{k=5}^{8} \phi^{(k)} \frac{h^{(k)}}{2} [-a_2^{to} a_1^{to}] \begin{bmatrix} \varphi_1^{(k)} \\ \varphi_2^{(k)} \end{bmatrix}_{to} \quad (2)$$

The primal nodes of the bottom plate element are connected to the primal nodes 1–4 of the interface element, and the primal nodes of the top plate are equal to the nodes 5–8 of the interface. The dual nodes of the interface element are numbered from 9 to 12. a_1^{to}, a_2^{to}, a_1^{bo}, a_2^{bo} are unit basic-vectors of the natural coordinate system ξ_α, which are situated in the reference planes of the connected plate elements. The location of the contact-plane can easily be calculated by simple vector-operations of the coordinates of the plate element nodes and the discrete corner thicknesses $h^{(k)}$. After transforming the surface-displacements $[u_i^*]_{bo}$ $[u_i^*]_{to}$ into the local coordinate system of the contact plane by using the normal unit vectors a_i^{co} we get

$$\begin{bmatrix} u_1^{co} \\ u_2^{co} \\ u_3^{co} \end{bmatrix}_{bo} = a^{to} \begin{bmatrix} u_1^* \\ u_2^* \\ u_3^* \end{bmatrix}_{bo} \quad ; \quad \begin{bmatrix} u_1^{co} \\ u_2^{co} \\ u_3^{co} \end{bmatrix}_{to} = a^{to} \begin{bmatrix} u_1^* \\ u_2^* \\ u_3^* \end{bmatrix}_{to} \quad (3)$$

with

$$a = [a_1^{co}|a_2^{co}|a_3^{co}] \quad (4)$$

The relative displacements between the points on the upper surface of the bottom element and the lower surface of the top element in the contact plane Δu_1^{co} and Δu_2^{co} (shear-stress-producing slip), and normal to the contact lane Δu_3^{co} (peel-stress-producing separation) read

$$\begin{bmatrix} \Delta u_1^{co} \\ \Delta u_2^{co} \\ \Delta u_3^{co} \end{bmatrix} = \begin{bmatrix} u_1^{co} \\ u_2^{co} \\ u_3^{co} \end{bmatrix}_{to} - \begin{bmatrix} u_1^{co} \\ u_2^{co} \\ u_3^{co} \end{bmatrix}_{bo} \quad (5)$$

or by means of the matrices Φ_{bo} and Φ_{to} containing the shape functions $\Phi^{(k)}$ for the system nodes $k = 1, 4$ and $k = 5, 8$

and the vectors u_{bo} and u_{to} containing the displacements u_i^{co} at the contact-reference plane we get

$$\begin{bmatrix} \Delta u_1^{co} \\ \Delta u_2^{co} \\ \Delta u_3^{co} \end{bmatrix} = a^T \Phi_{to} u_{to} - a^T \Phi_{bo} u_{bo} \quad (6)$$

These relative displacements are corresponding to the transverse tractions n_{13}, n_{23}, and n_{33}

$$n_{13} = k_{13} \Delta u_1^{co} \quad (7a)$$

$$n_{23} = k_{23} \Delta u_2^{co} \quad (7b)$$

$$n_{33} = k_{33} \Delta u_3^{co} \quad (7c)$$

Because there are two separated systems for the stiffener and the skin, delaminations can be modeled very easily by omitting the interface-element, or by reducing their spring-stiffnesses. This offers the possibility to regard to impact failures and delamination growth without having to change the finite element model. In order to capture the stress-peaks at the free edges of the stiffener flanges on the bond line, only one row of narrow elements is necessary.

Failure Criterion for Stiffener Debonding

For the calculation of the out-of-plane failure at the skin-stiffener interface, a criterion is applied which can be derived from the general quadratic polynomial stress tensor criterion

$$S_{ij}\sigma^{ij} + S_{ijkl}\sigma^{ij}\sigma^{kl} \leq 1 \quad (8)$$

by neglecting all coefficients which are independent from the normal direction. That leads to

$$S_{33}\sigma^{33} + S_{1313}(\sigma^{13})^2 + S_{2323}(\sigma^{23})^2 + S_{3333}(\sigma^{33})^2 \leq 1 \quad (9)$$

with the strength tensor coefficients

$$S_{33} = \left(\frac{1}{\sigma_{t.cr}^{33}} - \frac{1}{\sigma_{c.cr}^{33}}\right); \quad S_{3333} = \frac{1}{\sigma_{t.cr}^{33}\sigma_{c.cr}^{33}}$$

$$S_{1313} = \left(\frac{1}{\sigma_{cr}^{13}}\right)^2; \quad S_{2323} = \left(\frac{1}{\sigma_{cr}^{23}}\right)^2 \quad (10)$$

Most of the known debonding and delamination criteria can be derived from the above formulation with simplifying assumptions. With the assumed equivalence of tension and compression strengths the simplified criterion reads

$$\left(\frac{\sigma^{13}}{\sigma_{cr}^{13}}\right)^2 + \left(\frac{\sigma^{23}}{\sigma_{cr}^{23}}\right)^2 + \left(\frac{\sigma^{33}}{\sigma_{cr}^{33}}\right)^2 \leq 1 \quad (11)$$

Based on the transverse tractions calculated by the spring-type interface element Eq. (11) was further adapted to be applied to tractions instead of stresses:

$$\left(\frac{n^{13}}{n_{cr}^{13}}\right)^2 + \left(\frac{n^{23}}{n_{cr}^{23}}\right)^2 + \left(\frac{n^{33}}{n_{cr}^{33}}\right)^2 \leq 1 \quad (12)$$

The strength-values could be evaluated by a T-peel test specimen (Fig. 3) in the case of n_{cr}^{33}, and by conventional ILS-tests for n_{cr}^{13} and n_{cr}^{23}. As the peeling strength is mainly dependent on conditions concerning the matrix system and the curing process (fiber volume fraction, moisture content, and temperature), all the specimens for the evaluation of strength values were manufactured and tested under the same conditions as the stiffened plate specimens.

The application of Eq. (12) is only possible if the local transverse forces have been calculated by introducing a three-dimensional approach into the global plane-stress analysis of the whole structure. In the practical aircraft design, the stress engineer often has to handle very large finite element models for the calculation of the global structural response. In regard to the nonlinear analysis of the whole airframe structure, in some cases it might not be possible to further enlarge the system for the calculation of the peeling stresses. For this reason it could be very useful to have a failure criterion for debonding, which only refers to the postbuckled bending deformations. The magnitude of the peeling stresses depends on the stiffness relations between stringer and skin and can be assumed to be proportional to the bending strains, so a failure criterion on the basis of generalized bending strains is suggested

$$\frac{(\beta_{11})^2 + (\beta_{22})^2}{(\beta_{cr})^2} \leq 1 \tag{13}$$

This equation is only valid for stiffened panels with unloaded stiffeners. The critical value of β_{cr} has to be evaluated by peel-test specimens. In the performed calculations, a value of 0.28%/mm was used.

Tests and Test Results

Test Specimens

Fifteen specimens were tested in this investigation, manufactured from Thornell T300 8-harness graphite fabric and unidirectional tapes preimpregnated with Fibredux 913C epoxy resin. The typical elastic properties of three-dimensional lamina (T300/913C) are presented in Table 1.

With respect to maximum shear stiffness, the stacking sequence of the skin for all panels was chosen $[\pm 45]_5$, whereas, the stringer stiffnesses were varied by modifying geometry and stacking sequences (Table 2). This way the influence of different torsional and bending stiffness ratios between the skin and the stiffeners on the peeling effects could be studied. In order to avoid any crippling of stiffener parts and concentrating on the skin-stiffener interface, only T-shaped stringers were used with small flanges but high relative flange thicknesses. Stiffeners and skin were autoclave-cured in one shot, i.e, in the same way as it is practiced in the Airbus industry according to a modular design and manufacturing technique. Unidirectional tapes, as well as woven material, were used for the stiffener layups for investigating the influence of these combinations on the bonding strength of the skin-stiffener interface. In order to increase the bonding strength at two specimens, the interface was pinned with steel pins before curing. The pin-strengthened specimens had no stiffener debonding up to the failure load of the skin. Some four-point-bending tests done for control purposes as well as similar tests investigated by Richter,[15] showed that the bonding strength can be raised by a factor of about 3.0 when applying the pinning technique.

Material Properties

Two different peel-test specimens were used for the evaluation of interlaminar properties according to the two critical regions, one at the center of the skin-stringer bonding plane and the other one at the edge of the stiffener flange (Fig. 3).

A T-peel test specimen represents half the thickness of the stringer web angled to the flange which is joined to the skin laminate in a one-shot curing process. This specimen stands for a loading condition normal to the interface. Pop-off forces are produced in the postbuckling state by differences in bending stiffness between the stringer and the skin normal to the
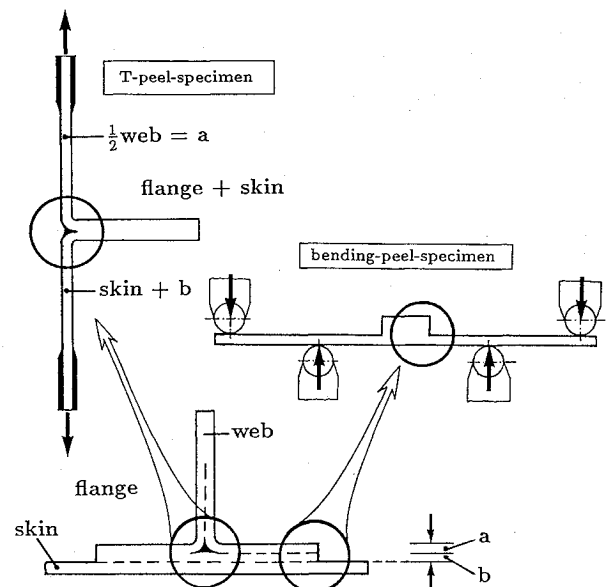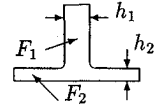

Fig. 3 Extraction of peel-test specimens.

Table 2 Stiffener characteristics

	Stiffener properties			
	$E_X I_X$, Nm²	$E_y I_y$, Nm²	GJ_D, Nm²	Test panel no.
$F_1 = [\pm 45_5, 0_6]_s$ $h_1 = [0.36_5, 0.25_6]_s$ $F_2 = [0_2, \pm 45_5]$ $h_2 = [0.25_2, 0.36_5]$	428	264	28.0	P_1 and P_2
$F_1 = [\pm 45_5, 0_6]_s$ $h_1 = [0.36_5, 0.25_6]_s$ $F_2 = [0_5, \pm 45_5]$ $h_2 = [0.25_5, 0.36_5]$	368	188	24.0	P_3
$F_1 = [(0/90)_5, 0_6]_s$ $h_1 = [0.36_5, 0.25_6]_s$ $F_2 = [0_5, (0/90)_5]$ $h_2 = [0.25_5, 0.36_5]$	1114	498	4.4	$P_4 \div P_8$
$F_1 = [(0/90), 0]_{4s}$ $h_1 = [0.36, 0.25]_{4s}$ $F_2 = [(0/90)_2, (0, 0/90)_4]$ $h_2 = [0.36_2, (0.25, 0.36)_4]$	1264	513	3.8	P_9
$F_1 = [0_{10}]_s$ $h_1 = [0.25_{10}]_s$ $F_2 = [0_{12}]$ $h_2 = [0.25_{12}]$	1798	724	3.9	P_{10} and P_{11}
$F_1 = [(0/90), 0]_{4s}$ $h_1 = [0.36, 0.25]_{4s}$ $F_2 = [0_2, (0, 0/90)_4]$ $h_2 = [0.25_2, (0.25, 0.36)_4]$	1330	558	3.9	P_{12} and P_{13}
$F_1 = [\pm 45_5, 0_6]_s$ $h_1 = [0.36_5, 0.25_6]_s$ $F_2 = [(0/90)_2, 0, \pm 45_5]$ $h_2 = [0.36_2, 0.25, 0.36_5]$	586	253	25.0	P_{14}

Table 1 Material properties for T300/913C

		UD-Tape	8H-Satin fabric
E_{11t}	GPa	127.0	69.0
E_{11c}	GPa	111.0	60.0
E_{22t}	GPa	8.5	64.0
E_{22c}	GPa	8.2	56.0
E_{33t}	GPa	8.5	8.5
E_{33c}	GPa	8.2	8.2
G_{12}	GPa	5.2	5.1
G_{13}	GPa	5.0	5.0
G_{23}	GPa	3.0	3.0
ν_{12}	——	0.28	0.28
ν_{13}	——	0.28	0.28
ν_{23}	——	0.47	0.47

axis of the stringer. Up to the initial failure, the T-test specimen is under pure peeling load, so that the evaluated failure load is a measure for the peeling strength. Table 3 shows the results of a series of T-peel tests. It should be noticed that the peeling strength is not rate independent. In the analytical study, a strength-value of 70 N/mm was used.

The second type of peel tests was performed by bending peel specimens, which represent the stress state at the edge of the stiffener flange when the skin buckles. Differences in bending and torsional stiffnesses between the skin and the stringer flange along the axis of the stiffeners cause shear and normal peel forces in the postbuckling state. The bending peel test specimens were used for the verification of the analytical model. Results are shown in Table 4.

Test Setup

The inplane shear testing of the stiffened panels was performed with the same picture-frame fixture that has been used in former investigations of the IFL with unstiffened flat plates[16] and shallow curved panels.[11] This shear-frame is composed of four pairs of back-to-back rigid steel edge members connected with high-strength pins. These pins are positioned with their centerlines coincident with the corners of the test section of the panel. By splitting the corner pins they do not extend through the test panel. Their location at the test section corners prescribes correct picture frame kinematics to insure proper shearing load introduction into the panel test section by applying a tension load along one diagonal of the frame. The specimen edges, which were clamped by the picture-frame

members, did not have any reinforcements and were prevented from sliding by added sandpaper.
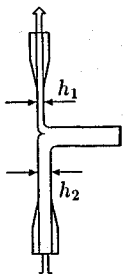
The tension load was applied by a 200 kN hydraulic testing machine, and the angle of shear of the loaded test specimens was determined by using several inductive displacement transducers for measuring both the elongation along the tension-diagonal and the shortening along the compression-diagonal. The initial geometric imperfections of the specimens and the out-of-plane buckling displacements along the compression-diagonal were monitored by a deflection transducer which was attached to a carriage running on a slideway. Electrical resistance strain gauge rosettes positioned on both surfaces of the specimens were used to measure normal and shear strains. The uniaxial tension loading of the picture-frame fixture was slowly applied in an incremental way up to the total failure of the specimen. At each load increment, the angle of shear, the out-of-plane displacements, and the strains at three significant positions were measured and recorded on magnetic tape. The stiffener separations could be monitored by optical inspections, or in one case, by ultrasonic scanning of the skin-stiffener interface region.

Test Results

The shear tests with single stiffened panels showed two different buckling modes depending on local imperfections and the bending and torsional stiffnesses of the stringers. If the bending stiffness of the stringer was low (stacking sequence ± 45 deg) the panel tended to buckle into a mode shape similar to that of an unstiffened panel with reduced amplitude in the stiffener area. This buckling mode can be regarded as symmetric to the center-point of the panel and is therefore indicated with an "s" at the following considerations. The next higher buckling mode could be observed when panels were tested with an increasing share of 0-deg layers in the stiffener cross section, which caused higher bending but reduced torsional stiffness. It is an antisymmetrical mode shape with sinusoidal amplitudes along both panel diagonals (indicated with an "a") and it tends towards a snapthrough into the first symmetric mode. This happened with one of the tests specimen (P_4) and could also be analytically proven. The results of all tests are listed in Table 5.

The debonding of the stiffener at the single-stiffened panels happened abruptly and totally with a loud popping noise. After the debonding, a tension field built up, and the specimen could further be loaded until final failure. But this final failure load was not very far above the stiffener debonding load (Table 5). The effect of the explosive stiffener debonding

Table 3 Results of T-peel test specimens

T-Peel test specimens (co-cured)	Stacking sequence 913C/T300	h_1, mm	h_2, mm	b, mm	Initial crack, P_{cr}/b, N/m
	h_1: $[\pm 45]_{3s}$				74.1 (V_1) $(s = 6.6)$
	h_2: $[\pm 45]_{4s}$ Fabric H8 Satin	2.1	3.0	30	63.0 (V_2) $(s = 16.5)$
	h_1: $[0/90]_{3s}$				64.1 (V_1) $(s = 3.12)$
	h_2: $[0/90]_{4s}$ Fabric H8 Satin	2.0	3.0	30	63.3 (V_2) (17.7)

V_1, Testing rate: 5.0 m/min. V_2, Testing rate: 0.5 mm/min. s, Standard deviation.
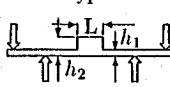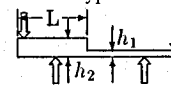
Table 4 Results of bending-peel tests

Bending-peel specimen (co-cured)	Type A	Type B
4-Point-bending test		
Quantity	8	9
Stiffness length L	45 mm	150 mm
Specimen width b	35 mm	40 mm
Thickness t_1	3.6 mm	2.1 mm
Thickness t_2	9.0 mm	8.0 mm
Specimen layup	$[0/90]_{5s}$	$[0]_8$
Flange layup	$[0/90]_{7s}$	$[0]_{11}$
Stiffness at t_1, $E \times I_X$	8.5 Nm²	3.9 Nm²
Stiffness at t_2, $E \times I_X$	253 Nm²	566 Nm²
Critical bending		
$m_{cr} = M_{cr}/b$	485 Nm/m	415 Nm/mm
Critical value of		
β_{cr}	0.28%/mm	0.30%/mm

Table 5 Summary of test results

Panel no.	h_m, mm	F_{cr}, kN	F_b, kN	τ_{cr}, N/mm²	τ_b, N/mm²	$F_{cr(Str.)}$, kN
	Unstiffened reference plate					
P_0	1.97	166	20	158	19	——
	Plates with one stiffener					
P_1	1.98	163	60	146	54	156
P_2	1.93	181	60	168	56	——
P_3	2.04	186	60	173	56	157
P_4	1.94	161	55	147	50	148
P_5	1.94	152	55	138	50	——
P_6	1.98	189	55	168	49	——
P_7	1.98	170	55	152	49	——
P_8	2.14	160	70	132	58	159
P_9	2.08	175	55	149	47	——
P_{10}	2.06	184	60	158	47	149
	Plates with two stiffeners					
P_{11}	2.20	189	70	151	56	159
P_{12}	2.38	——	75	——	56	——
P_{13}	2.30	184	60	142	46	144
P_{14}	2.27	182	55	142	43	158

can be seen as a result of a symmetric distribution of peeling stresses along the stringer bonding line, which is discussed in the next section.

Another type of mechanism could be observed at the double-stiffened region. So the failure mode at these panels was a partial delamination of one or both of the stringers starting at the unconnected ends and growing with increasing load. Most of the total debonding did not happen before the final failure of the whole panel.

Results and Discussion

Because the used fixture frame setup was very stiff compared to the tested panels, the engineering angle of shear γ was used as a loading parameter for comparison of experimental and analytical results, therefore making the consideration of the influences of friction of the frame-joint unnecessary. In the analysis, the load was introduced by shearing displacements (displacement-controlled), and during the tests the angle of shear was directly measured. As previously described, the out-of-plane displacements (buckling amplitude) were measured along the compression-diagonal of the test panel. Figure 4 shows such measurements for test panel P_4, which was the only specimen showing a "snap-through" from the second mode shape into the first one without stiffener debonding.

The slopes of the curves in the middle section show that the higher mode-shape causes a torsional deformation of the stringer with small bending, while the first mode-shape leads to a higher bending amplitude without any torsion. The total debonding of the stringer results in the formation of a diagonal tension field with double the amplitude. The panels with two stiffeners behaved much less dramatically in the test (Fig. 5). The partial debonding of one stiffener causes a slightly altering buckling mode shape with increasing amplitude at this panel section. The analytically determined out-of-plane deformations correlate well with the test results up to the initial failure. This can be seen in Figs. 6 and 7. Figure 6 representing test specimen P_6 (no stiffener debonding due to pinning), and Fig. 7 representing test specimen P_{10} with antisymmetrical mode
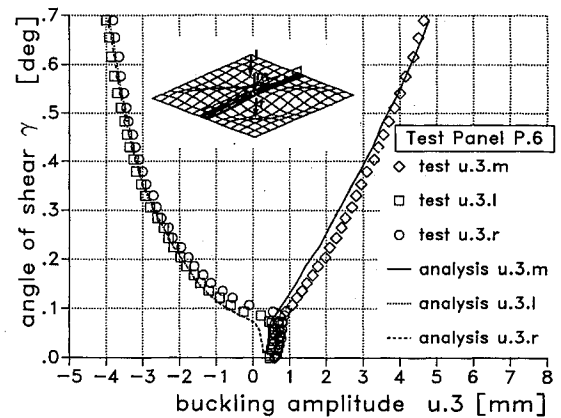

Fig. 6   Buckling amplitude as a function of shearing load for panel P_6 at three specific points.
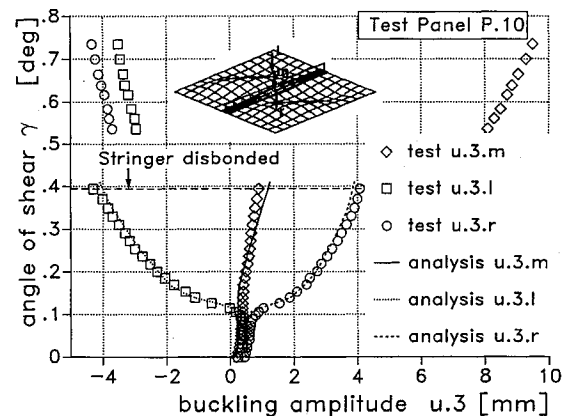

Fig. 7   Buckling amplitude as a function of shearing load for panel P_{10} at three specific points.
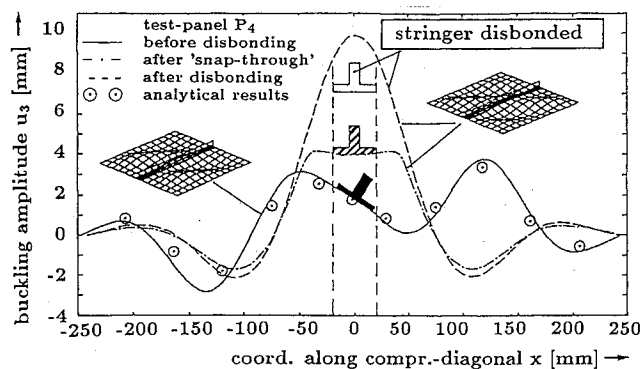

Fig. 4   Buckling amplitude along compression diagonal for test panel P_4 at three different load levels.
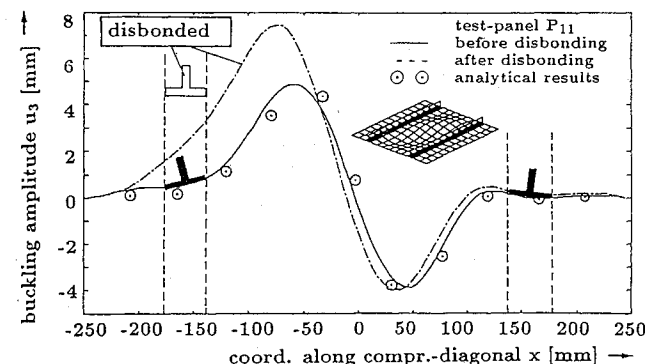

Fig. 5   Buckling amplitude along compression diagonal for test panel P_{11} at three different load levels.
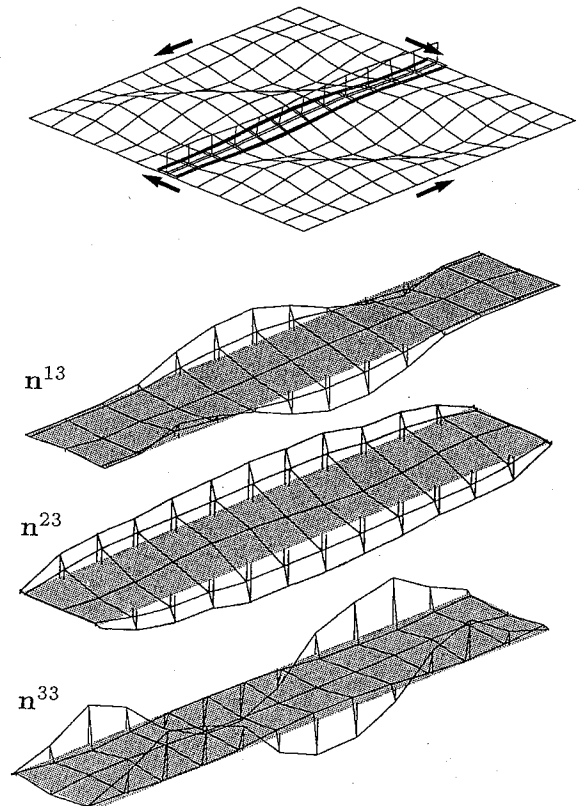

Fig. 8   Distribution of interlaminar tractions for a symmetric post-buckled mode shape.

shape and stiffener debonding at 0.4-deg shearing angle. The comparisons have been done for three specific points of the panel, one exactly at the center of the panel and the stringer (subscript $m \Rightarrow \nabla$) and one on the compression diagonal in the middle of the buckling field (left field: subscript $l \Rightarrow \odot$; right field: subscript $r \Rightarrow \diamond$). Differences in the prebuckled area are due to an incomplete idealization of the imperfections. In the analytical model a 1-cos-imperfection mode was assumed for the whole panel and overlayed by two separated 1-cos-modes for each field area.

Figures 8–10 show the results produced by the interface element. The transverse tractions n^{13}, n^{23}, and n^{33} have been plotted against each node line of the element mesh at the skin-stiffener interface section. For a better illustration, the mesh length in the direction of the transverse axis has been magnified by a factor of 2.5. The corresponding buckling mode shape can be seen on top of the figures. Figure 8 shows the results of the first mode shape. The n^{13}-distribution is directly affected by relative displacements normal to the stiffener axis and n^{23} by relative displacements along the stiffener axis. n^{13} reaches maximum values just at the location where the buckle transmits through the stringer section, while n^{23} achieves the maximum at the sections with the largest skin curvatures at the flanges of the buckle. The normal traction n^{33} is caused by the above-mentioned pop-off force at the center just beyond the stringer web, but it becomes negative (preventing the peeling) towards the free edges of the stringer flanges. The symmetry related to the center is obvious for all tractions at this mode shape.

If the panel buckles into the higher second-mode shape, the distribution of transverse tractions becomes quite different (Fig. 9). The n^{13} maxima are less significant and the n^{23} distribution is much more "filled," which seems to be the reason for a greater debonding sensitivity of this mode shape. Comparing the distributions of the two single-stiffened panels with those of the dual-stiffened ones (Fig. 10), it is easy to recognize that the maximum values are reached at the stiffener
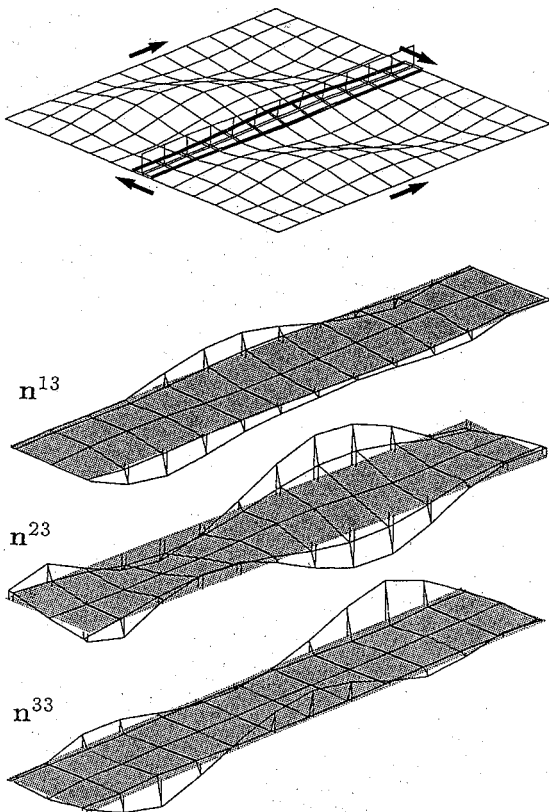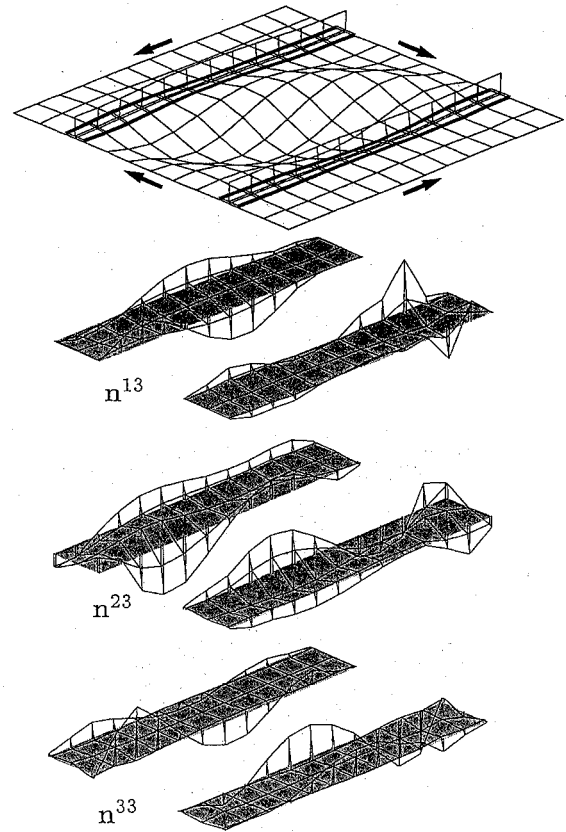

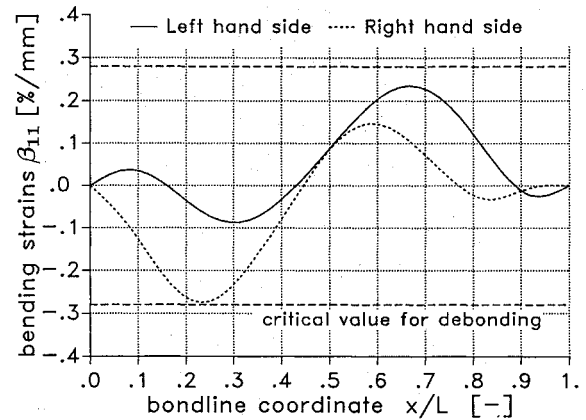Fig. 10 Distribution of interlaminar tractions at the dual-stiffened panels.

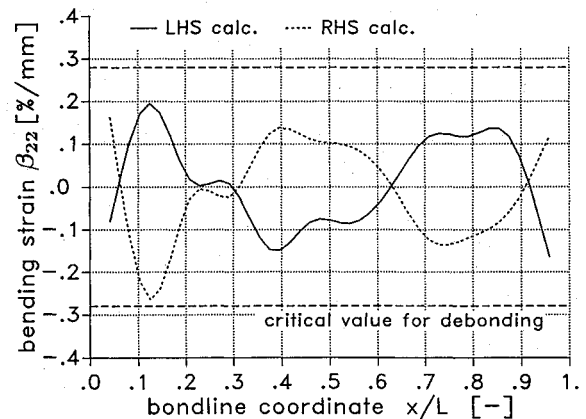Fig. 11 Distribution of generalized bending strain β_{11} along the stiffener bond lines.

Fig. 12 Distribution of generalized bending strain β_{22} along the stiffener bond lines.

Fig. 9 Distribution of interlaminar tractions for an antisymmetrical postbuckled mode shape.

edges near the tension diagonal of the panel. These are exactly the locations where the partial debonding of the stringers was initiated during the tests.

Figures 11 and 12 show the calculated distribution of the generalized bending strains along the stringer bond lines at both sides of the flanges and at a load level just before the debonding happened at the corresponding test specimen. The bending strains both reach the assumed critical value of 0.28%/mm, which means that they will satisfy the failure criterion formulated in Eq. (13). At this load level the alternative failure criterion [Eq. (12)] based on the interlaminar tractions is also satisfied.

Conclusions

An experimental and theoretical investigation was conducted to study the postbuckling response of flat-stiffened graphite-epoxy shear panels with special regard to the debonding failure characteristics due to postbuckled out-of-plane deflections. The test results have demonstrated the very high postbuckling load-carrying capacity of cocured stiffened panels under shear load in spite of the limitation caused by the stiffener debonding failure. There was no stiffener debonding below a load factor of at least 2.3 times the critical buckling load. An improvement of the stiffener peeling strength by transverse sticking will increase the debonding load up to a level which is higher than the ultimate load of the skin.

The presented analytical model proved to be capable for the analysis of the global nonlinear response as well as for the determination of the interlaminar effects at the skin-stiffener interface. The additional expenditure for the calculation of the three-dimensional stresses at the interface are small compared to an overall three-dimensional approach.

Because good correlations could be achieved between the analytical and the experimental results, the authors are encouraged to use the model for the analysis of stiffened panels under different loading conditions, e.g., compression or compression and shear. When compression loads are introduced into the panel, the stringer will carry part of the loading and this will increase the level of the peeling stresses related to the transverse shearing stresses. Therefore, the problem of stiffener debonding becomes even more significant with compression loading.

References

[1]Vestergren, P., and Knutsson, L., "Theoretical and Experimental Investigation of the Buckling and Post Buckling Characteristics of Flat Carbon Fibre Reinforced Plastics (CFRP) Panels Subjected to Compression or Shear Loads," International Council of Aeronautical Sciences, Paper B1-01, 1978, pp. 217–223.

[2]Kudva, N. J., and Agarwal, B. L., "Postbuckling Analysis of Stiffened Composite Shear Panels—Theoretical Analysis and Comparison with Experiments," International Council of Aeronautical Sciences, July 1981, pp. 221–229.

[3]Rouse, M., "Postbuckling and Failure Characteristics of Stiffened Graphite-Epoxy Shear Webs," AIAA Paper 87-0733, April 1987.

[4]Arnold, R. R., and Parekh, J. C., "Buckling, Postbuckling, and Failure of Stiffened Panels Under Shear and Compression," Journal of Aircraft, Vol. 24, No. 11, 1987, pp. 803–811.

[5]Bushnell, D., "Nonlinear Equilibrium of Imperfect Locally Deformed Stringer-Stiffened Panels Under Combined In-Plane Loads," Computers and Structures, Vol. 27, No. 4, 1987, pp. 519–539.

[6]Stein, M., "Postbuckling of Eccentric Open-Section Stiffened Composite Panels," International Council of Aeronautical Sciences, Paper 88-5.6.2, Sept. 1988, pp. 913–919.

[7]Sheinman, I., and Frostig, Y., "Post-Buckling Analysis of Stiffened Laminated Panel," Journal of Applied Mechanics, Vol. 55, Sept. 1988, pp. 635–640.

[8]Hyer, M. W., and Cohen, D., "Calculation of Stresses in Stiffened Composite Panels," AIAA Journal, Vol. 26, No. 7, 1988, pp. 852–857.

[9]Engblom, J. J., and Ochoa, O. O., "Finite Element Formulation Including Interlaminar Stress Calculation," Computers and Structures, Vol. 23, No. 2, 1986, pp. 241–249.

[10]Barsoum, R. S., and Freese, C. E., "An Iterative Approach for the Evaluation of Delamination Stresses in Laminated Composites," International Journal for Numerical Methods in Engineering, Vol. 20, No. 8, 1984, pp. 1415–1431.

[11]Wolf, K., and Kossira, H., "The Buckling and Postbuckling Behaviour of Curved CFRP Laminated Shear Panels," International Council of Aeronautical Sciences, Paper 88-3.4.3, Sept. 1988, pp. 920–930.

[12]Wolf, K., and Kossira, H., "Zur Berechnung des nichtlinearen Tragverhaltens von Strukturen aus Faserverbundwerkstoffen," Entwurf und Anwendung von Faserverbundstrukturen, Deutsche Gesellschaft für Luft- und Raumfahrt (DGLR), Rept. 87-02, 1987.

[13]Wolf, K., "Untersuchungen zum Beul- und Nachbeulverhalten schubbeanspruchter Teilschalen aus Kohlenstoffaserverstärktem Kunststoff," Ph.D. Dissertation, TU Braunschweig, Germany, 1988.

[14]Beer, G., "An Isoparametric Joint/Interface Element for Finite Element Analysis," International Journal for Numerical Methods in Engineering, Vol. 21, No. 4, 1985, pp. 585–600.

[15]Richter, H., "Querfestigkeit bei CFK-Strukturen," MBB Report Nr.: Z-142/87, Ottobrunn, Germany, 1987.

[16]Tunker, H., "Comparison of Measured and Computed Load-Deflection-Behaviour of Shear-Loaded Fiber Reinforced Plates in the Postbuckling Range," International Council of Aeronautical Sciences, Paper 84-3.4.3, Toulouse, France, Sept. 1984.